Metrics for the Quality of Footprint-Matched Passive Microwave Measurements

J. F. Galantowicz
Atmospheric and Environmental Research, Inc. (AER)
131 Hartwell Avenue
Lexington, MA 02421-3126
johng@aer.com

***Abstract*-In developing footprint matching schemes for the NPOESS (National Polar-orbiting Operational Satellite System) CMIS (Conical-scanning Microwave Imager Sounder) and ATMS (Advanced Technology Microwave Sounder) instruments, we have set up an array of tests for evaluating spatial weighting patterns, radiometric fidelity, and retrieval skill for composite passive microwave measurements. The purpose of the tests is two-fold. First, footprint-matching methods can be tuned to adjust both the degree of match to a target pattern and the level of composite measurement radiometric noise. Useful measures of each of these factors are needed in order to trade-off the benefits of each, complete the matching algorithm design, and run retrieval algorithms that use measurement error characteristics as a constraint. Second, environmental parameter retrieval skill depends on the quality of the footprint matching design, and we need to be able to evaluate what radiometric and spatial quality levels are optimal with respect to retrieval performance. To evaluate the diagnostic parameters, we simulated composite footprints from sensor patterns projected on a spherical-earth from a fixed satellite altitude. Spatial quality metrics include measures of fit to the target pattern, 3dB contour size, side-lobe level, proportional weight within the 3dB contour, and weight beyond specified linear boundaries (e.g., *X* km from center).**

Keywords-CMIS; ATMS; NPOESS; microwave radiometry; footprint matching; Backus-Gilbert

I. INTRODUCTION

Footprint matching has become commonplace for passive microwave data processing, with past applications to SSMI (Special Sensor Microwave/Imager), AMSU (Advanced Microwave Sounding Unit), and AMSR (Advanced Microwave Scanning Radiometer) [1][2][3]. We have developed footprint-matching algorithms for the NPOESS (National Polar-orbiting Operational Satellite System) CMIS (Conical-scanning Microwave Imager Sounder) [4] and ATMS (Advanced Technology Microwave Sounder) based on Backus-Gilbert optimization techniques [5][6]. The algorithms are designed to meet several objectives, including inter-channel footprint collocation and shape match, ATMS collocation to CrIS (Cross-track Infrared Sounder) fields-of-regard (FORs), correspondence to prescribed environmental data record (EDR) retrieval square cells (for CMIS), and composite brightness temperature (TB) radiometric noise minimization. However, the critical test is the ability of the composite TBs to reduce errors when used in geophysical retrieval algorithms, and ideally the footprint matching algorithms would be revised through end-to-end retrieval tests with high-resolution natural scenes. Although we are now in the process of building a simulation testbed for such tests, when complete it will be useful for retrieval error sensitivity tests but far too cumbersome for running iterative test and revision cycles for every footprint-matching scenario.

We have developed a set of footprint-matching spatial and radiometric noise metrics that are intended to rigorously evaluate the characteristics of TB composites. The goal is to provide practical measures of footprint matching performance that are independent of the natural scene and can be readily evaluated as footprint-matching algorithms are developed, tuned, and tested. The diagnostic parameters can aid selection of target patterns as well as help characterize the overall retrieval error budget. In this paper, we describe derivation of each metric, how it is useful, and general footprint matching algorithm practices that we have found to be helpful for reducing potential error sources.

II. FOOTPRINT MATCHING APPROACH

The footprint matching model builds a composite brightness temperature T_{Bc} from the coefficient a_i-weighted sum of contributing sensor TB samples, T_{Bi}:

$$T_{Bc} = \sum_{i=1}^{N} a_i T_{Bi} \ . \tag{1}$$

By definition, the a_i sum to 1 but some may be negative. The potential sample set can be thought of as all the sensor samples from a particular channel in a long section of the sensor swath. In practice, the set is smaller to eliminate the burden of zero or near-zero valued coefficients or in order to stabilize the algorithm's solution for the a_i. If the sensor noise σ_i is independent per sample i (which is not strictly true because of correlated noise from shared calibration samples), the composite sample noise is given by:

$$\sigma_c = \sigma_i \sqrt{\sum_{i=1}^{N} a_i^2} = \sigma_i \cdot SNF \tag{2}$$

where SNF stands for sample noise factor.

The composite footprint (or composite field-of-view, CFOV) is the a_i-weighted spatial superposition of all contributing sample footprints, $G_i(\rho)$:

$$G_c(\rho) = \sum_{i=1}^{N} a_i G_i(\rho) \tag{3}$$

where ρ is an earth coordinate vector and, in the general case, the G_i differ in both shape and location from each other and the reference footprint that we want G_c to match. To compute (3), we build earth-projected footprints on local regular grids for each sample, interpolated to a common reference grid, and compute the weighted sum at each point. We choose the sample grids to be large enough to cover all points with significant sensor gain. (Four-times the footprint 3dB field-of-

This work was supported by the NPOESS Integrated Program Office (NPOESS-IPO).

view—or FOV—size is usually sufficient with eight-times used in some cases for validation of results.) Each sample footprint is then normalized such that the integral over its local grid is 1, i.e.:

$$\iint_E dA G_i(\rho) = 1 . \tag{4}$$

Truncation of some sample grids where they fall off the reference grid requires that (4) be recalculated for G_c to confirm that all of the composite footprint weight has been accounted for. Off-grid excess weight is assigned to the appropriate spatial metrics defined below.

Before addressing analysis of the spatial properties of (3), we should briefly describe the method for generating the a_i using the Backus-Gilbert approach. (Details can be founding in [3], [4], and [5].) The a_i coefficient vector (length N) is given by:

$$\mathbf{a} = \mathbf{Z}^{-1}\left[\cos\gamma\,\mathbf{v} + \frac{1-\cos\gamma\,\mathbf{u}^{\mathrm{T}}\mathbf{Z}^{-1}\mathbf{v}}{\mathbf{u}^{\mathrm{T}}\mathbf{Z}^{-1}\mathbf{u}}\mathbf{u}\right] \tag{5}$$

where

$$\mathbf{Z} = \mathbf{G}\cos\gamma + \mathbf{E}\,w\sin\gamma . \tag{6}$$

G is the N x N symmetric matrix whose elements represent the overlap between sampled footprints:

$$\mathbf{G}_{ij} = \iint_E dA G_i(\rho) G_j(\rho) \tag{7}$$

where E is the earth grid. The N-elements of vector **u** are always equal to 1 here due to normalization of $G(\rho)$ (4). The elements of vector **v** represent the overlap between each sampled footprint and a reference footprint, G_r:

$$v_i = \iint_E dA G_i(\rho) G_r(\rho) . \tag{8}$$

The tuning coefficient γ in (6) balances composite sample noise and spatial match in the minimization cost function. (**E** is the error covariance matrix of the N samples but we can set it to the identity matrix, **I**, without loss of generality when independent sample noise is assumed; w is then chosen to equalize with the magnitude of **G**.). With γ=0, (5) minimizes spatial match (resolution) without regard for noise based on the cost function:

$$Q_R = \iint_E dA\left[G_r(\rho) - \sum_{i=1}^{N} a_i G_i(\rho)\right]^2 . \tag{9}$$

Setting γ=0 can yield a low-noise coefficient set but it is not guaranteed due to sensor footprint irregularities (even when G_r has a large FOV size). Also, inversion of the matrix **Z** can be numerically noisy due to round-off errors when symmetry causes rows of **G** to be similar. For the cross-track scanning ATMS—whose scan pattern is symmetric along track but with strong asymmetry along-scan due to the increase in FOV size with scan angle—we added a step for iterative optimization of both γ and N, with the N samples in each iteration chosen from those ranked highest in terms v_i. With up to 25 N and 38 γ values examined at each of 30 CrIS scan positions, it was impractical to use full 2-D analysis of G_c in this process and so intermediate spatial tests were used. We performed full analysis only on the final γ-N selections.

Although (8) and (9) allow for any reference footprint $G_r(\rho)$, the solution to (5) is more stable with respect to γ and N choice when the optimum value of (9) is not large. Also, to meet the objective of inter-channel co-registration, we need to choose a G_r that the algorithm can fit all channels to with similar success. For example, the main lobes of CMIS and ATMS footprints are approximately 2-D elliptical-Gaussian shapes with second-order features due to side-lobes and sensor motion during the sample integration period. If G_r is chosen to be a top-hat shape falling to zero along sharp edges—or even a smoother Gaussian shape but with smaller FOV size than the some sensor footprints—significant mismatch error will remain in (9) for any a_i set. To minimize mismatch error, our approach has been to base G_r on elliptical-Gaussian or modified sensor footprints and, where appropriate, to also include along-scan convolution either to mimic sample integration (ATMS) or to reach a desired along-scan FOV size (CMIS). We have attempted resolution enhancement—that is, choosing a G_r with FOV size smaller than the sensor—only on an experimental basis. As discussed below, we plan to test G_r trade decisions for both TB estimation and retrieval skill using a high-resolution simulation testbed.

III. Composite Footprint Quality Metrics

Composite footprint analysis includes evaluation of both radiometric and spatial metrics. The key radiometric metric is SNF (2), but we also calculate a second metric—calibration noise factor—that accounts for calibration-induced correlated noise:

$$CNF(N_c) = \sqrt{\frac{1}{N_c}\sum_{i=1}^{N} a_i^2 + \frac{2}{N_c}\sum_{i=1}^{N-1}\sum_{j=i+1}^{N} a_i a_j\left(1 - \frac{\delta_{ij}}{N_c}\right)} \tag{10}$$

where N_c is the number of scans over which calibration data is averaged and δ_{ij} is the smaller of the number of scan lines separating samples i and j or N_c. The total composite sample variance is then given approximately by:

$$(\Delta T_c)^2 = \sigma_T^2\left(SNF^2 + \frac{1}{k}CNF^2\right) \tag{11}$$

where k is the number of warm-load calibration samples and σ_T is a single-sample radiometric noise (NEDT) for both earth-scene and warm-load observations.

We calculated intermediate spatial metrics used during the tuning process only along two orthogonal cuts (e.g., along-and cross-scan) through the reference footprint center. (The metrics are quicker to evaluate plus they only require computation of (3) along the cuts.) For primary fit analysis we used two metrics: (a) the mean absolute deviation to the reference footprint over distances equal to two times the reference FOV size in each direction, and (b) the root-mean-square deviation over the same distances. Although metric (b) is closer to the cost function (9), we concluded that (a) more accurately captures the effect mismatches would have in brightness temperature estimation. We also calculated the composite footprint FOV size along each cut as a secondary confirmation of fit results. The FOV size can be a poor measure of fit where the observations are undersampled (samples spaced farther apart than half the FOV size) or where there are second-order footprint spatial irregularities.

A third important fit metric during tuning would measure side-lobe levels. In tuning ATMS composites, we concluded that coefficient sets with any negative a_i should be excluded in order to eliminate composite footprint side-lobes and regions with negative weight, which could be difficult to interpret in retrievals. However, where side-lobes are allowed there is a trade between side-lobe level and main-beam resolution that increases the ambiguity in any simple definition of footprint

resolution. Without side-lobes, footprint weight that falls beyond the main-beam FOV is concentrated near it and decreases monotonically away from it. With side-lobes, some of that weight is (presumably) transferred to within the FOV and the rest to more distant regions. Our hypothesis is that larger single-lobe footprints will produce better, more consistent retrievals than smaller FOV footprints with side-lobes. And although a high-resolution testbed can test that conjecture for specific scenes, we believe the overall robustness of retrievals to scene spatial heterogeneity is improved when footprint weight is concentrated in one place.

Following algorithm tuning, we conduct full 2-D analysis of G_c at selected scan positions. (Smooth behavior of SNF and the intermediate spatial metrics across all scan positions validates the more limited 2-D analysis.) First, visual inspection of the composite footprint contours (Fig. 1) reveals obvious side-lobes or FOV mismatch. We then compute the following metrics for each composite 2-D footprint:

1) Absolute fit error relative to the reference footprint:

$$F = \iint_E dA \left| G_r(\rho) - \sum_{i=1}^{N} a_i G_i(\rho) \right| \qquad (12)$$

2) Square root of the squared error relative to the reference footprint (i.e., (9)):

$$F_2 = sqrt\left(\iint_E dA \left[G_r(\rho) - \sum_{i=1}^{N} a_i G(\rho) \right]^2 \right) \qquad (13)$$

3) Along-scan and cross-scan FOV size: Calculated as the size of the smallest rectangle inscribed by the composite footprint 3dB contour.

4) Center-of-weight along-scan and cross-scan offset from the reference footprint center of weight: The center-of-weight is calculated from points within the footprint 3dB contour. The reference footprint center of weight is not at the beam peak at oblique incidence angles and the composite footprint peak is a poor measure of the center especially if undersampling results in rippling across the center of the footprint.

5) Weight WITHIN 3dB contour of reference footprint: Total composite footprint weight integrated over the 3dB contour of the reference footprint, expressed as a percentage. This is an integral similar to (4) but only including the specified region. For comparison, the weight within the 3dB contour for a circular Gaussian reference footprint is only about 50%.

6) Maximum weight BEYOND coastline 1: The maximum total composite footprint weight integrated separately over four regions tangent to the reference FOV. That is, if Y_r, X_r are the reference footprint cross-scan and along-scan FOV sizes, then the four regions are demarcated by $y>Y_r/2$, $y<Y_r/2$, $x>X_r/2$, and $x<X_r/2$ and can be thought of as the footprint weight falling across a linear coastline. Large values indicate that either the composite FOV is much larger than the reference or that the composite has side-lobe-like spatial features. Also includes the "off-grid" weight. For comparison, the weight for a circular Gaussian reference footprint is about 14%.

7) Maximum weight BEYOND coastline 2: Same as above only the four regions are farther from the footprint center: $y>Y_r$, $y<Y_r$, $x>X_r$, and $x<X_r$. Also includes the "off-grid" weight. For comparison, the weight for a circular Gaussian reference footprint is about 2%.

8) Maximum side-lobe level: Value of any local maxima beyond the 3dB contour in terms of gain relative to the footprint peak.

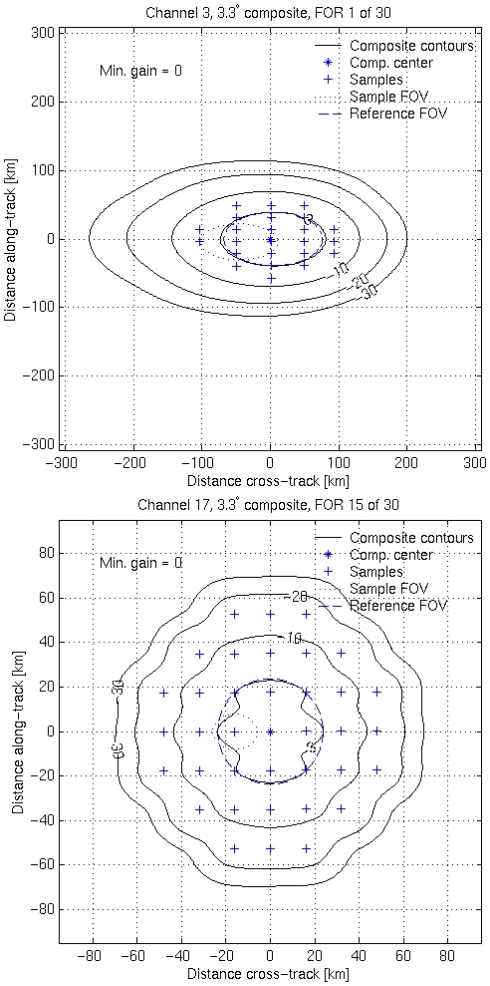

Figure 1. Example composite contour plots for ATMS channels 3 (top) and 17 at CrIS FORs 1 and 15. Contours are plotted at -3, -10, -20, and -30dB. Also plotted: Composite footprint center of weight (*) (reference footprint is located at plot origin), locations of each contributing ATMS sample (+), an example ATMS 3dB contour, and the reference footprint 3dB contour.

Fig. 2 plots the final composite footprint metrics for ATMS channels 3, which has a nominal instantaneous beamwidth of 2.2° and has been matched to a 3.3° static (i.e., not elongated by scan motion) circular-Gaussian beam footprint. SNF and the fit metrics are fairly consistent across the scan with some scatter due to scan-position dependent footprint size, second-order characteristics, and tuning. The footprint weight metrics (within 3dB and beyond coastlines 1 and 2) are very close to the values obtained for a circular Gaussian footprint. Side-lobe levels are negligible meaning that the footprint weight decreases monotonically away from the 3dB contour. Shifts in the center-of-weight are small compared to the FOV size.

We matched ATMS channel 17, which has a 1.1° nominal beamwidth, to the same reference footprint as channel 3 (Fig. 3). The critical weight metrics (including those not shown in Fig. 3) are similar to channel 3 across the entire scan. The main differences are the lower SNF and fact that the fit error metrics (e.g., absolute error) peak at the center of scan. This is the result of undersampling, as shown in Fig. 1, which produces rippling across the composite footprint even though the reference FOV size is closely matched.

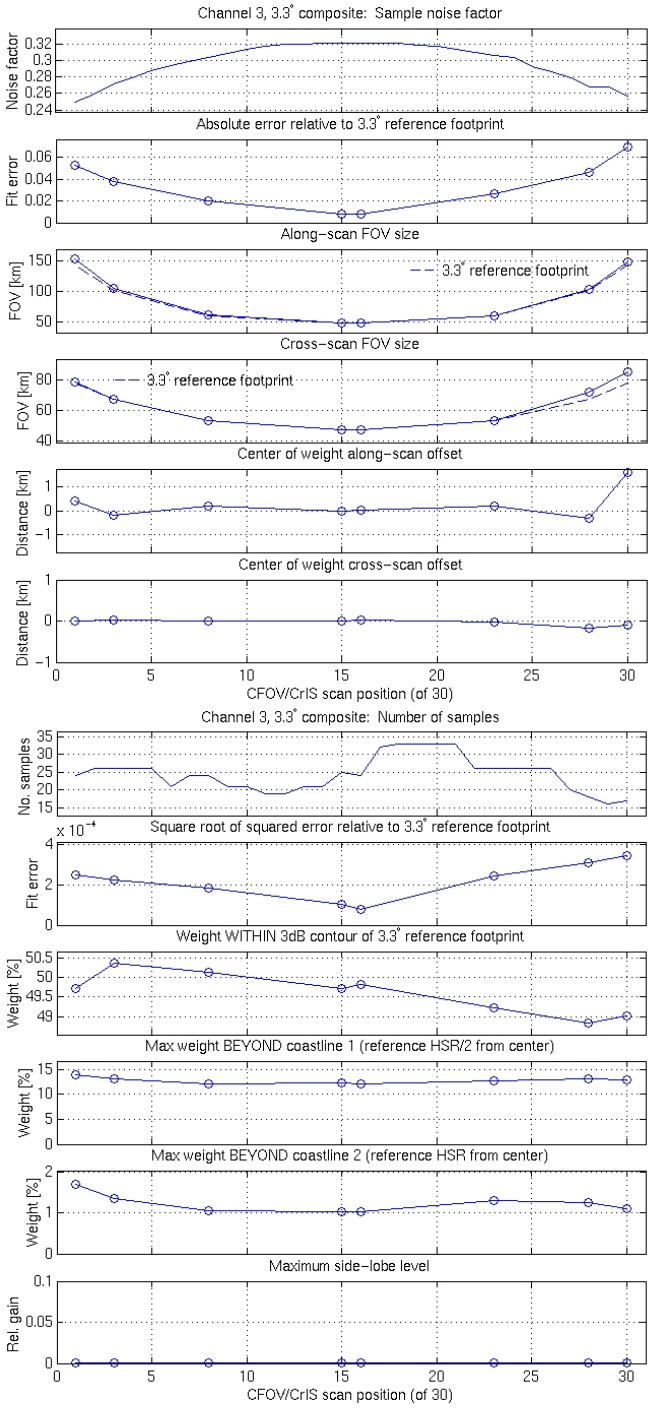

Figure 2. 2-D composite footprint analysis for ATMS channel 3.

IV. Conclusion

In this paper, we have presented a set of radiometric and spatial tests useful for evaluating composite brightness temperature sample quality. Without a capability for complete end-to-end analysis of retrieval error impacts it is not possible to objectively optimize composite sample noise and spatial characteristics with regard to environmental parameter retrieval skill. For end-to-end retrieval evaluation, we are developing a 3-D, high-resolution (~3 km) simulation testbed

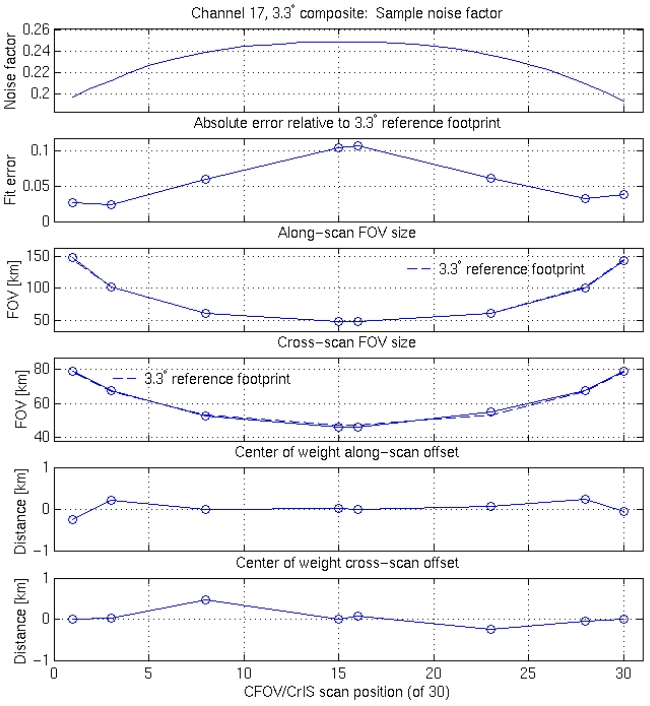

Figure 3. 2-D composite footprint analysis for ATMS channel 17.

based on numerical weather model fields and simulated surface parameters (e.g., emissivities). The testbed will allow evaluation of the CMIS footprint-matching algorithm and retrieval performance under controlled, well-characterized conditions that allow specific error sources to be isolated, evaluated, and minimized. However, even with this capability intermediate spatial analyses are needed for quicker composite footprint evaluation during footprint matching algorithm tuning. Our plan is to use the testbed to establish composite sample radiometric and spatial quality goals based on the metrics described here and then define and tune the footprint-matching algorithm separately to achieve those goals. The testbed can also provide another tier of radiometric spatial fidelity tests for final analysis of composite footprint characteristics.

References

[1] R. L. Armstrong and M. J. Brodzik, "An Earth-gridded SSM/I data set for cryospheric studies and global change monitoring," *Adv. Space Res.*, 16(10):155-163, 1995.

[2] R. Bennartz, "Optimal Convolution of AMSU-B to AMSU-A," *J. Atm. Oceanic Tech.*, 17(9):1215–1225, 2000.

[3] P. Ashcroft and F. J. Wentz, *ATBD AMSR Level 2A Algorithm*, RSS Tech. Report 121599B-1, 2000.

[3] J. F. Galantowicz, T. Nehrkorn, R. Hoffman, and A. Lipton, *ATBD for the CMIS EDRs, Vol. 1: Overview, Pt. 2: Footprint Matching*, AER Inc., 2001, http://www.npoess.noaa.gov/Library/ATBD_index.html.

[4] A. Stogryn, "Estimates of brightness temperatures from scanning radiometer data," *IEEE Trans. Ant. and Prop.*, AP-26(5):720-726, 1978.

[5] G. A. Poe, "Optimum interpolation of imaging microwave radiometer data," *IEEE Trans. Geosci. Rem. Sens.*, 28(5):800-810, 1990.